Accepted Manuscript

Effects of crab burrows on pore water flows in salt marshes

Pei Xin, Guangqiu Jin, Ling Li, David Andrew Barry

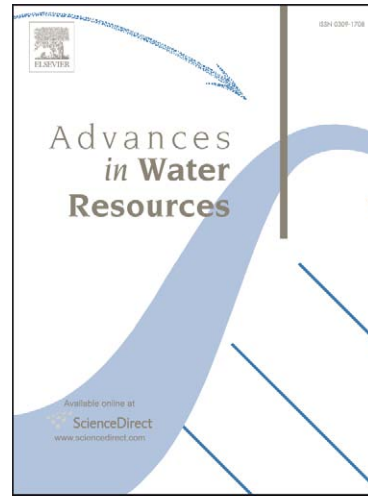

PII: S0309-1708(08)00230-3
DOI: 10.1016/j.advwatres.2008.12.008
Reference: ADWR 1378

To appear in: *Advances in Water Resources*

Received Date: 30 October 2008
Revised Date: 22 December 2008
Accepted Date: 24 December 2008

Please cite this article as: Xin, P., Jin, G., Li, L., Barry, D.A., Effects of crab burrows on pore water flows in salt marshes, *Advances in Water Resources* (2009), doi: 10.1016/j.advwatres.2008.12.008

Effects of crab burrows on pore water flows in salt marshes

Pei Xin[1,2,#], Guangqiu Jin[1], Ling Li[2], David Andrew Barry[3]

[1]Centre for Eco-Environment Modelling, Hohai University, Nanjing, China

Email: xinpei1980@163.com

jingq02@126.com

[2]School of Engineering, The University of Queensland, Queensland, Australia

Email: l.li@uq.edu.au

[3]Laboratoire de technologie écologique, Institut des sciences et technologies de l'environnement, Ecole Polytechnique Fédérale de Lausanne, Station 2, CH-1015, Lausanne, Switzerland

Email: andrew.barry@epfl.ch

Re-submitted to *Advances in Water Resources*, 22 December 2008

[#] Author to whom all correspondence should be addressed. Tel: +86 (25) 8378-6919. Fax: +86 (25) 8378-6919

Abstract

Macro-pores such as crab burrows are found commonly distributed in salt marsh sediments. Their disturbance on the soil structure is likely to influence both pore water flows and solute transport in salt marshes; however, the effects of crab burrows are not well understood. Here, a three-dimensional model simulated tidally driven pore water flows subject to the influence of crab burrows in a marsh system. The model, based on Richards' equation, considered variably saturated flow in the marsh with a two-layer soil configuration, as observed at the Chongming Dongtan wetland (Shanghai, China). The simulation results showed that crab burrows distributed in the upper low-permeability soil layer, acting as preferential flow paths, affected pore water flows in the marsh particularly when the contrast of hydraulic conductivity between the lower high-permeability soil layer and the overlying low-permeability soils was high. The burrows were found to increase the volume of tidally driven water exchange between the marsh soil and the tidal creek. The simulations also showed improvement of soil aeration conditions in the presence of crab burrows. These effects may lead to increased productivity of the marsh ecosystem and enhancement of its material exchange with coastal waters.

Key words: Coastal wetland; Plant growth; Numerical modelling; Preferential flow; Richards' equation; Tidal forcing

1. Introduction

Salt marshes are important intertidal wetlands vegetated by herbs, grasses and/or low shrubs [3,7,35]. Bordered with tidally dynamic coastal water bodies, salt marshes are affected by various physical and biogeochemical processes that are associated with periodic submersions of marsh soils by the tidal water. Among these processes, subsurface flow and solute transport largely determine the marsh soil condition and material exchange with coastal waters [9,31,33,36]. The plant's rhizosphere is within the intertidal zone, which undergoes cycles of immersion and emersion driven by the tides. This leads to complex aeration conditions (for root aerobic respiration), which are crucially important for plant growth [3,7,9,23]. Furthermore, the tidal inundation induces solute exchange across the marsh soil-water interface, which in turn influences the material budget of coastal water ecosystems [34].

Recent hydrological studies on salt marshes based on numerical simulations focused on the pore water circulation near tidal creeks. These studies have demonstrated links of tidally driven subsurface flows with both marsh soil aeration and solute exchange [13,21,33,39]. The simulation results suggested that during early stages of tidal submergence, surface water infiltrates almost vertically through the marsh platform and decreases the soil aeration condition. The marsh soils may then become depleted in oxygen. Such a condition would impact the plant root respiration and hence plant growth [28]. As the tide recedes, a considerable amount of pore water seeps out of marsh sediments near the creek bank. In contrast, little drainage takes place in the marsh interior. Therefore, the optimal soil aeration condition tends to occur near the tidal creek. These simulation results seem to give an explanation for previous observations that salt marsh plants such as *Spartina alterniflora* often grow better near tidal creeks than in the inner areas [9,23]. The flow dynamics with dominant infiltration through the marsh platform and drainage across the creek bank lead to a net pore water flow in the form of circulation near the creek (Fig. 1). This pore water circulation at the local scale provides a mechanism for more rapid solute exchange between the marsh soil and the tidal creek than that given by diffusive processes through the marsh surface. The circulation ultimately affects the overall material exchange between the marsh and coastal water.

Among the previous numerical studies, the Richards' equation-based model of Ursino et al. [33] showed that if the soil's saturated hydraulic conductivity was relatively low (less than 10^{-6} m/s), an unsaturated zone away from the creek would persist below the soil surface even after the tide had flooded the marsh platform. Wilson and Gardner [38] pointed out that the boundary conditions adopted by Ursino et al. [33] in their numerical simulations were unrealistic. However, Li et al. [21] also revealed this persistent unsaturated zone in simulations using a two-phase model and more realistic boundary conditions. Furthermore, they showed that the Ursino et al. [33] model could over-predict infiltration in areas with trapped air. In other words, the persistent unsaturated zone away from the creek could be more extensive than that calculated by Ursino et al. [33]. Such permanently aerated zones would allow a prolonged presence of oxygen for aerobic root respiration of local plants in the marsh system.

These modelling studies [21,33,39] were all based on homogeneous soils. In reality, most marshes possess soil strata. Commonly, low-permeability mud or silt loam are found to overlie sands or sandy deposits in marsh systems, for example, the marsh at Carter Creek in Virginia [17], the Manukau Harbour marsh in New Zealand [10], the Tomago South wetlands in Australia [19], the North Inlet basin in Carolina [12] and the Bahía Blanca Estuary in Argentina [27]. Gardner [15] reported perhaps the first numerical study on tidal dynamics of pore water flows in heterogeneous marsh soils with a two-layer structure – a sand (high-permeability) layer underlying a mud (low-permeability) layer. The study examined the effects of the soil structure on the spatial distribution and volume of seepage from marsh soils to the tidal creek. Simulation results showed that the total seepage from the mud-sand marsh to the creek is larger than that from a muddy marsh. The underlying sand layer enhances the pore water circulation through the marsh. As the contrast of hydraulic conductivity between the lower (sand) and upper (mud) layer increases, the total seepage from the mud-sand marsh increases nonlinearly. The findings of this study also imply that the presence of an underlying sand layer with a higher permeability leads to lowering of the water table in the upper mud layer during the ebb tide and hence improves local aeration conditions.

The other type of marsh soil heterogeneity is due to macro-pores produced by invertebrates commonly found in salt marshes. For example, crab burrows are typically distributed in marsh sediments [5,12,19,24,27]. The presence of invertebrates has implications for biogeochemical processes in marsh sediments. Through burrowing and feeding activities, the invertebrates are known to increase sediment-water interface (surface area exposed to overlying water or air) and mixing between pore water and overlying surface water, thus affecting chemical reactions and transport in marsh sediments [1,20]. Previous studies of marsh subsurface flows have developed hypotheses about the roles of macro-pores like crab burrows. Nuttle [26] considered that the saturated hydraulic conductivity of the marsh soil is controlled by its macro-pore structure, which is itself biotically controlled. Montalto et al. [25] further suggested that preferential flow may be facilitated by macro-pores. These hypotheses were tested indirectly by Harvey and Nuttle [18] through tracer experiments.

Despite these previous studies, the effects of macro-pores on the marsh system and underlying mechanisms are not fully understood. With considerable disturbance on the soil structure, how crab burrows may affect pore water flows and associated soil aeration conditions in the marsh remains an important question; as discussed above both factors control a large extent the soil's biogeochemical condition and hence plant growth. To address this question, we conducted a field investigation on a salt marsh at the Chongming Dongtan wetland (Shanghai, China) where a sandy loam layer with relatively high hydraulic conductivity underlies a surface mud layer, similarly to the model configuration considered by Gardner [15]. However, the difference is that, at this field site, there is a relatively large number of crab burrows down to the bottom of the upper mud layer (around 60 cm below the marsh surface). While the reason why the crabs tunnel to this depth is unclear, the burrows penetrating the mud layer may act as preferential flow paths for water. These burrows may change not only the behaviour of pore water flows but also associated aeration conditions and solute exchange in the marsh soil. For example, the permanently unsaturated zones suggested by Ursino et al. [33] may not exist in marsh soils in the presence of crab burrows. Moreover, the pore water circulation demonstrated by previous studies [13,15,21,33] is likely to be altered by widespread macro-pores like crab burrows.

The aim of this study is to develop a three-dimensional model to investigate pore water flows in marsh soils affected by crab burrows. The model was based on a simplified tidal marsh configuration using data collected from the Chongming Dongtan wetland. In the model, a low-permeability soil layer overlies a high-permeability soil layer. Crab burrows were distributed in the upper soil layer according to the measured density at the field site. Numerical simulations were conducted to generate insight into effects of crab burrows on pore water flows and associated water exchange, soil aeration and tidal signal propagation under different conditions of varying hydraulic conductivity contrast between the lower and upper soil layer (K_{lower}/K_{upper}).

2. Field investigation

The field site is located at the Chongming Dongtan wetland (between 31°25´ ~ 31°38´ N and 121°50´ ~ 122°05´ E) on the eastern part of the Chongming island (Shanghai, China), the largest island in the Yangtze delta area (Fig. 1a). The tidal flats at the site are dominated by various marsh plants, such as *Phragmites australis*, *Scirpus mariqueter* and *Spartina alterniflora* [11]. The Yangtze estuary experiences semidiurnal and mixed tidal fluctuations with a maximum range around 4.64 m [8]. The tidal signal is attenuated significantly due to friction as it propagates along the tidal creek at the study site and exhibits high degree of asymmetry with a much more rapid rising phase than falling phase. During spring tides, the maximum range of creek water level fluctuations at the study site is about 1.0 m (mainly depending on the elevation of the creek bottom). For this condition, the local marsh platform is inundated at high tide with a water depth around 0.1 m (this depth varying with the marsh topography, wind and vegetation coverage).

As discussed in the introduction, macro-pores such as crab burrows are a dominant feature of soils in the intertidal zone. At the field site, burrows near creeks are often dug by *Uca arcuata* (crab species shown at the lower left corner of Fig. 1b). According to our observations, the crabs can dig burrows up to 10-cm deep in no more than 2 h without interference. We collected data at the site during a neap tide (9 July 2007). Along a cross-creek transect (dashed line in Fig. 1b), 109 crab burrows of diameters between 1 and 2 cm were found over an area of 14 m ×1.5 m. The areal burrow density (number of burrows per square meter area) for this size range was 5.2/m^2. Another 68 crab burrows of diameters between 2 and 4 cm were also found. The corresponding areal burrow density was 3.2/m^2. There were many smaller burrows not included in the survey. These burrows are likely to have less important effects on the pore water flow compared with those described already. Therefore, these small burrows were neglected in the study.

The morphological structures of these burrows were determined by means of polyester resin casting, a technique often used in the marine industry [4,32]. At low tide, randomly selected burrows were filled with resin. The polyester resin is denser than seawater and can harden even in wet conditions; therefore, water inside the burrow was pumped out before pouring the resin in order to create a complete cast of the burrow. The cast was later excavated by hand and with small shovels after resin solidified, and then cleaned and examined.

When the burrow casts were excavated, the difference in soil texture between two layers was evident. Black, odoriferous soils were found underneath the 60-cm surface mud layer (Fig. 1c, varying spatially and temporally). Soil samples were collected from each layer and later analysed in the laboratory for the hydraulic conductivity (falling head method), porosity (oven drying) and particle size distribution (laser diffraction particle analysis). The soil particle size distribution ranged from 0.36 μm to 140.58 μm. The soils from the lower layer contained larger particles than the upper layer soils. The average hydraulic conductivity and porosity of the upper soils were determined to be 1.18×10^{-6} m/s and 0.51, respectively (6 soil samples), and 6.25×10^{-6} m/s and 0.51 respectively for soils from the lower layer (also 6 samples). Such a layered soil structure was the focus of Gardner's [15] numerical study on pore water flows in heterogeneous marsh soils. The crab burrows distributed extensively at the field site represent important, additional heterogeneity of marsh soils. According to our measurements, the average length of the burrows is about 40 cm. Nearly half of the surveyed burrows are, however, longer than 60 cm with the maximum length reaching 70 cm (Fig. 1d). Deep burrows penetrate through the upper soil layer and may act as preferential flow paths, affecting pore water flows and associated aeration conditions in marsh soils.

Crab burrows were not distributed regularly in the marsh; nor did they possess regular shapes (Fig. 1d). Moreover, the dimensions of the burrows varied both spatially and temporally due to crabs' continuing activities of burrowing and feeding. Therefore, it is difficult to deploy pressure transducers in these burrows to measure water pressure fluctuations in response to tides. Quantitative analyses based on mathematical models with precise information about burrows (location, size and layout) would not be feasible as it is impractical to acquire such information and use it to create the mesh required by the simulations. Here, we adopted an alternative approach by developing a representative model of the marsh system with simplified configurations assuming vertical burrows of a constant length (equal to the thickness of the upper soil layer) and regular distribution in the upper soil layer (Fig. 1e). This approach reflects key features of the marsh system and serves the purpose of the study to examine general effects of crab burrows as potentially important preferential flow paths.

3. Conceptual and mathematical models

3.1. Physical conditions

Based on the field site configuration, the three-dimensional model developed here was assumed to lie between two parallel tidal creeks and extend in the along-creek (y) direction by a width of $W = 0.5$ m (Fig. 1e). The model domain, with a simplified geometry as indicated by the central vertical cross-section **ABCDEFG** (reference point coordinates are given in Table 1), reflects the topography of the field site. **DE** shows the marsh platform and **AG** is for the impermeable base. **BD** represents the creek bank with a slope similar to that of the creek profile measured at the field site. No creek bottom section is present in the model, i.e., a triangular creek cross-section was assumed (based on the configuration at the field site). The domain is divided into two zones (Zone A and Zone B shown in Fig. 1e) separated by a horizontal interface **CF** at the depth of 0.6 m from the marsh platform.

Crab burrows were assumed to be distributed along the centreline of the model domain as shown in Fig. 1e and penetrate straight through the upper soil layer (Zone A). The spatial interval of crab burrows L was set to 0.5 m, giving an areal crab burrow density of 4/m^2. Because not all measured burrows were deep enough to penetrate the upper soil layer, the burrow density set in the model was approximately half of that measured at the field site. To generate a 3-D rectangular finite-element mesh that can be used in SUTRA (the modelling software used in the study), each crab borrow was assumed to be a cube with the size of 4 cm × 4 cm × 60 cm. The size of simulated burrows reflects the upper end of the size range measured in the field.

For the purpose of comparison with previous modelling work [15,21,33], we adopted a sinusoidal tide as the forcing condition in the model instead of using the measured tidal signal at the field site, i.e.,

$$h(t) = Z_{MSL} + A\cos(\omega t), \tag{1}$$

where $h(t)$ is the water level in the creek [L], t is the time [T], Z_{MSL} is the mean water level in the creek [L], A is the amplitude of tide-induced water level oscillations in the creek [L] and ω is the tidal angular frequency [T^{-1}].

In all simulations, the same tide with amplitude of 0.5 m and period of 12 h ($\omega = \pi/6$ rad/h) was set. The mean creek water level was set to 1.6 m, which allowed the marsh platform to be inundated with a water depth of 0.1 m at high tide.

3.2. Mathematical description and numerical method

The variably saturated pore water flow in the marsh soil is governed by Richards' equation:

$$\nabla \bullet \left[K(\psi) \nabla \Phi \right] = \frac{\partial \theta}{\partial t}, \tag{2}$$

where Φ is the total hydraulic head, and $\Phi = \psi + z$ [L]; ψ is the capillary pressure head [L]; z is the elevation [L]; $K(\psi)$ is the relative hydraulic conductivity [L/T]; and θ is the volumetric moisture content, $= \phi S_w$ (ϕ is the soil porosity and S_w is the soil saturation). The relationship between the hydraulic conductivity, soil saturation and capillary pressure head is given below according to Gardner [16]:

$$K(\psi) = K_S \exp(\alpha \psi), \tag{3}$$

$$S_w = (1 - S_{Wres}) \exp(\alpha \psi) + S_{Wres}, \tag{4}$$

where K_S is the saturated hydraulic conductivity [L/T], α is the inverse of the mean capillary rise [L^{-1}] and S_{Wres} is the residual water saturation.

It is worth recalling that Richards' equation is valid when pressure gradients in the air phase are insignificant compared with those in the water phase. Due to the large viscosity difference between air and water, this condition is reasonable except when the air becomes trapped [21]. For all the cases modelled in the present study, no persistent unsaturated zone with air trapped was present due to crab burrows which provide the means for air to be easily displaced. Therefore, the use of Richards' equation is appropriate.

We assumed constant pore water density in the model, which is consistent with measurements of small density variations at the field site. Also we neglected in equation (2) the change of aquifer storage due to the compressibility of fluid and soil matrix. The standard formulation of the compressibility terms is based on the assumption of constant total stress on the porous medium and hence $\Delta\sigma$ (change of effective stress) = $-\Delta P$ (change of pore water pressure). When the salt marsh is flooded at high tides, fluctuations of pore water pressure with varying depth of overlying water would lead to changes of effective stress under the assumption of constant total stress, generating an artificial pressure wave through the elastic soil. However, the total stress on the marsh soil is not constant during flooding and varies in the same way as the pore water pressure, thus giving invariant effective stress (i.e., no expansion or contraction of soil matrix). To account for the total stress variation and remove the artificial pressure wave, a tidal loading term needs to be incorporated into Richards' equation with the standard compressibility formulation [29]. Our numerical tests showed that if the saturated hydraulic conductivity of soils is large than 10^{-6} m/s, the compressibility plays a negligible role in governing the pore water flow in the marsh soil. Therefore, an alternative, simpler approach is to neglect the compressibility terms in the governing equation, in which case the tidal loading modification is no longer required [29]. This approach is valid only if the effect of fluid and solid compressibility on the pore water flow in the marsh soil is negligible [14].

Crab burrows were included in the model as highly conductive zones with saturated hydraulic conductivity K_s = 10 m/s and porosity ϕ= 1. This enables simulations of the burrows' rapid responses to tidal water level fluctuations. Numerical tests showed that as long as the hydraulic conductivity of the burrows is set high enough (≥ 10 m/s), its value does not affect the simulation results. Similar techniques have been previously used in groundwater models to simulate dynamic conditions induced by surface water [2,22,30].

The governing equation was solved using the SUTRA code, a 3-D finite element computer program that simulates partially saturated, variable-density fluid flow, and solute or energy transport in porous media [37]. Modifications of the code were made in order to implement the tidally influenced boundary condition along the creek bank (boundary **BD**) and marsh platform (boundary

DE).

3.3. Initial and boundary conditions

The initial condition was set according to the hydrostatic pressure determined by the water level at the high tide. All the simulations were run for a relatively long period to ensure that the numerical solutions reached a quasi-steady state (i.e., periodic solutions unaffected by the initial condition).

Boundaries **AB**, **AG** and **EG** together with two side-boundaries in the along-creek direction were treated as no flow boundaries. SUTRA was modified to simulate the tidally dynamic boundary condition along the creek bank (**BD**) and marsh platform (**DE**). A subroutine was set up to determine the state of each node on these boundaries at every time step. On the marsh platform, the nodal heads were prescribed by hydrostatic pressure given by depth of overlying water. These nodes switched to no-flux boundaries in the absence of overlying water. In SUTRA, the pressure-prescribed boundary condition was implemented by connecting the boundary node to a "reservoir" with specified pressure through a "conduit" of very large conductance. This method gives a simple switch between each boundary condition type by setting the conductance to zero when the zero-flux condition applies. Similarly, the tidally dynamic boundary condition was implemented along the creek bank, allowing also for the development of a seepage face defined by the rule: If the nodes above the tidal water level were saturated at the previous time step, they were taken as seepage face nodes with the atmospheric pressure [39].

3.4. Parameters values used in the simulations

The parameter values used in the base simulation were set to reflect the field conditions at the study site. The soil porosity was 0.51 for both layers. The hydraulic conductivities of upper and lower soils were 1.18×10^{-6} m/s and 6.25×10^{-6} m/s, respectively. The inverse of mean capillary rise and residual saturation were 1 m^{-1} and 0.3 respectively for both upper and lower soils. Although these values were not directly from measurements, they are consistent with the soils types encountered at the field site [6]. Values of other model parameters concerning the simulation domain, burrows and tidal forcing have been given in §3.1.

To compare with the base simulation, a set of numerical experiments were conducted to examine the effects of crab burrows on pore water flows in salt marshes under different soil layer conditions. The hydraulic conductivity of the lower layer was varied between 1.18×10^{-6} m/s and 6.25×10^{-5} m/s, giving a range of hydraulic conductivity contrast between the two soil layers with K_{lower}/K_{upper} varying from 1 to 53, thereby considering a range from a homogeneous soil to one with a large hydraulic conductivity contrast.

For all simulations, the SUTRA code was run with a time step of a minute. The same mesh generated with 135,408 nodes and 120,600 elements was used in all cases. Typically, the burrow zones were refined so that each burrow was represented by 240 elements. Tests on the simulation's independence of time step and mesh size were conducted. The results based on the present model setting were found to agree well with those from models with a further refined mesh and smaller time step. In other words, the results presented here are considered to be converged numerical solutions to the mathematical model.

4. Simulation results and discussions

4.1. Effects on pore water flow dynamics

The simulated pore water flow is generally three-dimensional, especially in areas near the crab burrows. However, due to symmetry, the flow on the vertical plane along the model's centreline (**ABCDEFG**) is two-dimensional. Since key flow characteristics are expected to be two-dimensional in the vertical and creek-normal direction, the discussion below will first focus on such two-dimensional flows. For the purpose of comparison, reference simulations were also conducted without crab burrows distributed in the marsh.

Simulation results show that for the base condition, the pore water flow velocities at high tide were very low in both cases (with and without burrows included; Fig. 2a). This indicates that the pore water pressure in the marsh soil was largely hydrostatic. No unsaturated zone was present in either case.

As the tide receded, pore water flow developed within 10 m from the creek. The flow activity was weakened with increasing distance from the creek, consistent with the attenuation of associated tidal groundwater waves (Fig. 2b). Overall the flow rate in the upper soil layer was small due to the relatively low hydraulic conductivity. Significant downward flows appeared at the lower end of the burrows near the interface between the two soil layers, suggesting that the burrows acted as preferential flow paths and enhanced locally the drainage of the upper soils with collected water discharging to the lower soil layer. This effect can be seen more clearly in Fig. 3 where flow velocities are plotted for two observation points in the upper layer near the burrow next to the creek: one between the burrow and the creek (left hand side of the burrow), and the other landward of the burrow (right hand side of the burrow). The flows at both observation points were affected significantly by the burrow when compared with the result from the reference simulation (without the burrows). During the ebb tide (between elapsed time 4 and 8 h), the horizontal flow velocity at the left hand side observation point reversed its direction while the magnitude of the vertical flow velocity was reduced significantly (Fig. 3a in comparison with Fig. 3c). On the right hand side, the horizontal flow velocity increased slightly with a relatively large reduction of the vertical flow for this period (Fig. 3b in comparison with Fig. 3d). These changes of local flow patterns indicate that considerable water from the upper soil layer was drained into the lower layer through the burrows.

At the low tide, the flows were intensified in both cases (Fig. 2c). As the outflow area moved towards the low tide limit, the characteristics of dominant vertical and horizontal flows in the upper and lower layers respectively became pronounced, and so did the effect of crab burrows on the flows.

On the rising tide, inflow (from the creek to the marsh soil) occurred below the intersection of the tidal water level with the creek bank (Fig. 2d). Relatively large upward pore water flows developed near the lower end of the burrows, suggesting that the burrows again acted as preferential flow paths. Since the tidal signal propagated more quickly in the lower more permeable layer, the presence of the burrows with "large hydraulic conductivity" could lead to leakage of tidal energy to the upper layer.

At the beginning of the flooding over the marsh platform, the flow velocities at the observation points on both sides of the near-creek burrow surged (Fig. 3). This indicates that the overtopping water irrigated quickly the burrows and subsequently flowed into the surrounding marsh soils. This has implications for the behaviour of local soil water saturation and aeration condition as discussed further in §4.3.

Focussing on the area around the burrow next to the creek, we examined flows on the *y*-*z* plane across the centre of the burrow, which demonstrate the flow's three-dimensionality (Fig. 4). The effects of the burrow on flows in the *y* and *z* direction (Figs. 4a-c) were similar to those discussed above (Figs. 4e-g). In essence, the burrow acts like a drain for the upper soils during the ebb tide and a recharge well during the rising tide. However, the drainage effect seems to be more pronounced as indicated by the averaged flows over the tidal cycle (Figs. 4d and h; further discussion on the averaged flows is given below).

4.2. Effects on water exchange between marsh soils and creek

Previous studies have suggested that the tide induces pore water circulation near the creek with surface water infiltrating through the marsh platform and discharging from the creek bank. To examine effects of crab burrows on the pore water circulation, we averaged the simulated pore water flows over a tidal cycle. The tidally averaged flows exhibited circulation patterns as expected for both cases (Fig. 5). While net inflow occurred over the upper part of the creek bank and across the marsh platform, net outflow concentrated between the bank's intersection with the soil layer interface and the low tide limit. The overall water passage was characterised by downward movement through the upper soils followed by seaward flow in the lower soil layer prior to discharge to the creek. Increased average downward flows at the bottom of the crab burrows again indicated preferential flow paths through these burrows, which enhanced downward water movement in nearby areas. This may result in increase of the overall circulation rate and hence exchange between the marsh soil and the creek.

Based on the average flow velocities, we calculated the difference between the total volume of inflow and outflow across the creek bank over a tidal cycle. This quantity represents the net exchange between the marsh soil and the creek. The net exchange was 0.015 m^3 (0.030 m^3 per meter distance along the creek) for the case with crab burrows and 0.014 m^3 (0.028 m^3 per meter distance along the creek) without crab burrows. The presence of crab burrows led to a slight increase of the net exchange by 3.5%. Although the effect is small for the simulated base condition, the enhancement of exchange may become more significant with increased burrow density and hydraulic conductivity contrast between the soil layers. A series of simulations were conducted with the hydraulic conductivity contrast between the layers varying as described above.

Simulation results showed that for a homogeneous soil (K_{lower}/K_{upper} = 1), the tide-induced water exchange was only slightly affected by crab burrows. Although the burrows had much higher hydraulic conductivity than that of the soil, they occupied a very small volume of the medium and thus by themselves affected little the overall pore water flow. As K_{lower}/K_{upper} increased, the total water exchange volume increased for both cases with and without crab burrows in a similar fashion (Fig. 6). However, the increase of exchange for the marsh system with crab burrows was more substantial. The relative difference of total water exchange volume between the two cases was calculated and found to increase with K_{lower}/K_{upper}. The effects of crab burrows on the pore water flow and exchange in the marsh were intensified as the hydraulic conductivity contrast between the two soil layers increased. Compared with the homogeneous configuration, the additional water exchange induced by crab burrows was 15.4% for K_{lower}/K_{upper} = 53. This hydraulic conductivity contrast is not uncommon in natural salt marshes [15].

4.3. Effects on soil aeration conditions

To examine effects of crab burrows on water saturation in the marsh soil, we focussed on the area near the burrow next to the creek on the vertical plane along the centreline. Results from the base condition simulations are shown in Fig. 7. The marsh soil was largely fully saturated except for the near-surface area where the saturation varied with the tidal stage. At high tide, the marsh soil was fully saturated (result not shown). As the tide receded, the near-surface soil became partially saturated in both cases with and without the burrow (Figs. 7a and f). However, the presence of the burrow led to further reduction of the saturation around it with a down-coning profile evident (Fig. 7a). This is consistent with the drainage effect of the burrow on the pore water flow in the upper soil layer as discussed in §4.2. This effect was intensified as the low tide approached (Fig. 7b). On the rising tide, the saturation profile rebounded (Fig. 7c) due to increase of hydraulic head in the burrow in response to the tide that propagated through the lower soil layer more quickly than in the upper layer. As the tidal water level rose just above the marsh platform, the flooding water filled the burrow immediately and subsequently infiltrated the soil around the burrow over the depth, resulting in increase of local saturation to 100% (Fig. 7d).

The opposing effects of the burrow on local soil saturation during the rising and falling tide were not even. Tidally averaged soil saturation profiles showed that overall the burrow reduced local soil saturation (Fig. 7e). The reduction was relatively small for the base condition. However, more pronounced effects were observed in simulations with a large hydraulic conductivity contrast between the layers, as shown in Fig. 8 for K_{lower}/K_{upper} = 53. On average, the depth of partially saturated zone increased due to the presence of crab burrows. A reduction of local soil saturation occurred in areas around all crab burrows although the effects were attenuated with increasing distance from the creek. This reduction of soil water saturation may be linked to improvement of soil aeration and hence plant growth.

4.4. Effects on pore water pressure fluctuations

The effects of crab burrows on pore water flow and soil water saturation as discussed above are fundamentally due to burrow-induced modifications of the pore water pressure (hydraulic head) field. To examine such modifications, we again focussed on the area around the burrow next to the creek where the burrow effects were the most profound. Pore water pressure (head) distributions underneath the burrow were first examined. Results showed pressure increase and decrease around the burrow's centre on the falling and rising tide, respectively (compare Figs. 9a,b with Figs. 9c,d). These pressure profiles correspond to significant outflow from and inflow to the burrow previously observed near the lower end of the burrow on these tidal stages (Fig. 4).

We also examined the hydraulic head fluctuations at two observation points: one inside the burrow (Fig. 10a) and the other underneath (Fig. 10b). The hydraulic head at the observation point inside the burrow declined more quickly with the receding tide compared with the signal from the reference simulation (without burrows). The opposite trend, however, was found at the observation point underneath the burrow, which exhibited a slower decline of the hydraulic head as the tide receded. These results are consistent with the local flow characteristics – the burrows collected pore water in the upper layer and discharged it into the lower layer. The other distinctive modification of the hydraulic head behaviour by the burrow was the instantaneous rise of the head to the tidal water level at the instant of flooding over the marsh platform at both observation points, suggesting immediate filling of the burrow by the flooding water. The subsequent changes of local soil saturation, which have been discussed in the above section, suggest that if crab burrows exist in the marsh sediments, the persistent unsaturated zones identified previously [33] may not exist in the marsh soils due to increased surface water irrigation through the burrows during overtopping.

5. Conclusions

Crab burrows are a common feature of many salt marshes. Their effects on enhanced dispersion and bioturbation in marshes have been studied previously. Here, we have developed a three-dimensional model to examine a new mechanism by which crab burrows may affect significantly the marsh system in the exchange of the coastal water and the atmosphere. The Richards' equation-based model simulates tidally driven, variably saturated pore water flow in the marsh soil along with the disturbance due to crab burrows.

In parallel with numerical modelling, we have carried out a field investigation with measurements of crab burrow density, distribution and size at the Chongming Dongtan wetland (Shanghai, China). The marsh soil at the field site is characterised by a two-layer structure, also a common feature of salt marshes: an upper mud layer (low hydraulic conductivity) and a lower sandy loam layer (high hydraulic conductivity). Many of the surveyed burrows were found to penetrate the upper mud layer and could potentially be preferential flow paths between the two soil layers.

Model simulations based on field measurements and a wider range of conditions demonstrated that crab burrows acted as a drain for the upper soil layer during the ebb tide and a recharge well on the rising tide. However, the opposing effects did cancel each other out but instead resulted in an increase of pore water circulation across the marsh soil-water interface and reduction of average soil water saturation at shallow depths. Increased pore water circulation may lead to enhancement of solute exchange between the marsh soil and tidal creek, and prevent overly high pore water solute concentrations. At the same time, reduced soil water saturation is likely to improve soil aeration. Therefore the presence of crab burrows is likely to be in favour of the plant growth and hence increase the productivity of salt marshes.

Although we have not been able to measure the simulated crab burrow effects in our preliminary field investigation, the modelling study has provided important insight into the physical processes. A large hydraulic conductivity contrast between the shallow and deep soil layers has been found to be an essential factor that underpins the role of crab burrows in modifying the conditions and behaviour of water flow in salt marshes. The characteristics of pore water pressure under the influence of crab burrows revealed here will provide a base for designing future experimental studies on crab burrow effects. It will be a challenge to collect detailed data of hydraulic head fluctuations in and around crab burrows at the field site to validate model predictions. More complex models are needed to study further the effects of crab burrows coupled with other factors including the marsh topography (e.g., a vertical creek bank), multiple tidal constituents (e.g., spring-neap tides), long period seasonal water level oscillations, precipitation and evapotranspiration. Furthermore, the effects caused by temporal and spatial variations in burrow sizes and their distribution may also be important for pore water flows in salt marshes. All these challenges present useful directions for future investigations on salt marshes.

Acknowledgments

This research has been supported by the National Natural Science Foundation of China (50425926), Australian Research Council (DP0772660) and Postgraduate Discovery Project Grant of Jiangsu Province, China (CX07B_132z).

References

[1] Aller RC. Transport and reactions in the bioirrigated zone. Oxford: Oxford Press, 2001.

[2] Anderson MP, Hunt RJ, Krohelski JT, Chung K. Using high hydraulic conductivity nodes to simulate seepage lakes. Ground water 2002; 40: 117–22.

[3] Armstrong W. Waterlogged soils. Hoboken NJ: John Wiley, 1982.

[4] Atkinson RJA, Chapman CJ. Resin casting: A technique for investigating burrows in sublittoral sediments. Progress in Underwater Science 1984; 9: 15–25.

[5] Botto F, Iribarne O. Effect of the burrowing crab Chasmagnathus granulate (Dana) on the benthic community of a SW Atlantic coastal lagoon. Journal of Experimental Marine Biology and Ecology 1999; 241: 263–284.

[6] Carsel RF, Parrish RS. Developing joint probability distributions of soil water retention characteristics, Water Resources Research 1988; 24: 755–769.

[7] Chapman VJ. Salt marshes and salt deserts of the world. London: Leonard Hill, 1960.

[8] Chen JY. The integrated investigation report on the resource in the Shanghai coast and tidal flats. Shanghai: Shanghai Academic Press, 1988.

[9] Dacey JWH, Howes BL. Water uptake by roots controls water table movement and sediment oxidation in short Spartina marsh. Science 1984; 224: 487–489.

[10] Dolphin TJ, Hume TM, Parnell KE. Oceanographic processes and sediment mixing on a sand flat in an enclosed sea, Manukau Harbour, New Zealand. Marine Geology 1995; 128:169–181.

[11] Gao ZG, Zhang LQ. Multi-seasonal spectral characteristics analysis of coastal salt marsh vegetation in Shanghai, China. Estuarine, Coastal and Shelf Science 2006; 69: 217–224.

[12] Gardner LR, Porter DE. Stratigraphy and geologic history of a southeastern salt marsh basin, North Inlet, South Carolina, USA. Wetlands Ecology and Management 2001; 9: 371–385.

[13] Gardner LR. Role of geomorphic and hydraulic parameters in governing pore water seepage from salt marsh sedi-

ments. Water Resources Research 2005; 41: W07010. doi:10.1029/2004WR003671.

[14] Gardner LR, Wilson AM. Comparison of four numerical models for simulating seepage from salt marsh sediments. Estuarine Coastal and Shelf Science 2006; 69: 427–437.

[15] Gardner LR. Role of stratigraphy in governing pore water seepage from salt marsh sediments. Water Resources Research 2007; 43: W07502. doi:10.1029/2006WR005338.

[16] Gardner WR. Some steady state solutions of unsaturated moisture flow equations to applications to evaporation from a water table. Soil Science 1958; 82: 228–232.

[17] Harvey JW, Germann PF, Odum WE. Geomorphological control of subsurface hydrology in the creek bank zone of tidal marshes. Estuarine, Coastal and Shelf Science 1987; 25: 677–691.

[18] Harvey JW, Nuttle WK. Fluxes of water and solute in a coastal wetland sediment. 2. Effect of macropores on solute exchange with surface water. Journal of Hydrology 1995; 164: 109–125.

[19] Hughes CE, Binning P, Willgoose GR. Characterisation of the hydrology of an estuarine wetland. Journal of Hydrology 1998; 211: 34–49.

[20] Kristensen E. Impact of polychaetes (Nereis spp. and Arenicola marina) on carbon biogeochemistry in coastal marine sediment: A review. Geochemical Transactions 2001; 2: 92–104.

[21] Li HL, Li L, Lockington D. Aeration for plant root respiration in a tidal marsh. Water Resources Research 2005; 41: W06023. doi:10.1029/2004WR003759.

[22] Mao X, Enot P, Barry DA, Li L, Binley A, Jeng DS. Tidal influence on behaviour of a coastal aquifer adjacent to a low-relief estuary. Journal of Hydrology 2006; 327: 110–127.

[23] Mendelssohn IA, McKee KL, Patrick WH. Oxygen deficiency in Spartina alterniflora roots: Metabolic adaptation to anoxia. Science 1981; 214: 439–441.

[24] Minkoff DR, Escapa M, Ferramola FE, Maraschín SD, Pierini JO, Perillo GME, Delrieux C. Effects of crab-halophytic plant interactions on creek growth in a S.W. Atlantic salt marsh: A Cellular Automata model. Estuarine, Coastal and Shelf Science 2006; 69: 403–413.

[25] Montalto FA, Steenhuis TS, Parlange JY. The hydrology of Piermont Marsh, a reference for tidal marsh restoration in the Hudson river estuary, New York. Journal of Hydrology 2006; 316: 108–128.

[26] Nuttle, WK. The extent of lateral water movement in the sediments of a New England salt marsh. Water Resources Research 1988; 24: 2077–2085.

[27] Perillo GME, Minkoff DR, Piccolo MC. Novel mechanism of stream formation in coastal wetlands by crab–fish–groundwater interaction. Geo-Marine Letters 2005; 25: 214–220.

[28] Pezeshki SR. Wetland plant responses to soil flooding. Environmental and Experimental Botany 2001; 46: 299–312.

[29] Reeves HW, Thibodeau PM, Underwood RG, Gardner LR. Incorporation of total stress changes into the ground-water model SUTRA. Ground Water 2000; 38: 88–99.

[30] Robinson C, Li L, Barry DA. Effect of tidal forcing on a subterranean estuary. Advances in Water Resources 2007; 30: 851–865.

[31] Silvestri S, Marani M. Salt-marsh vegetation and morphology: Basic physiology, modelling and remote sensing observations. Washington: AGU monograph, 2004.

[32] Stieglitz T, Ridd P, Müller P. Passive irrigation and functional morphology of crustacean burrows in a tropical mangrove swamp. Hydrobiologia 2000; 421: 69–76.

[33] Ursino N, Silvestri S, Marani M. Subsurface flow and vegetation patterns in tidal environments. Water Resources Research 2004; 40: W05115. doi:10.1029/2003WR002702.

[34] Valiela I, Teal JM. The nitrogen budget of a salt marsh ecosystem. Nature 1979; 280: 652–656.

[35] Vernberg FJ. Salt-marsh processes: A review. Environmental Toxicology and Chemistry 1993; 12: 2167–2193.

[36] Visser EJW, Colmer TD, Blom CWPM, Voesenek LACJ. Changes in growth, porosity, and radial oxygen loss from adventitious roots of selected mono- and dicotyledonous wetland species with contrasting types of aerenchyma. Plant, Cell & Environment 2000; 23: 1237–1245.

[37] Voss CI, Provost AM. A model for saturated-unsaturated, variable-density ground-water flow with solute or energy

transport, U.S. Geological Survey. Water-Resources Investigations Report 02-4231, 2002.

[38] Wilson AM, Gardner LR. Comment on “Subsurface flow and vegetation patterns in tidal environments” by Nadia Ursino, Sonia Silvestri, and Marco Marani, Water Resources Research 2005; 41: W07021, doi: 10.1029/2004WR003554.

[39] Wilson AM, Gardner LR. Tidally driven groundwater flow and solute exchange in a marsh: Numerical simulations. Water Resources Research 2006; 42: W01405. doi:10.1029/2005WR004302.

Notation

A	tidal amplitude [L]
H	crab burrow depth [L]
$h(t)$	tidal water level at time t [L]
K_{lower}/K_{upper}	hydraulic conductivity contrast between the lower and upper soil layer
K_S	saturated hydraulic conductivity [L/T]
$K(\psi)$	relative hydraulic conductivity [L/T]
L	interval of crab burrows [L]
S_W	water saturation
S_{Wres}	residual water saturation
t	time [T]
W	width of the modelled salt marsh [L]
x	distance from the tidal creek [L]
y	distance along the tidal creek [L].
z	elevation [L]
Z_{MSL}	mean sea level [L]
α	inverse of the mean capillary rise [L^{-1}]
ω	angular frequency [T^{-1}]
ψ	capillary pressure head [L]
θ	water content

568 **Table 1**. Coordinates of reference points of the model domain (*x*, *z*).

A (m)	**B** (m)	**C** (m)	**D** (m)	**E** (m)	**F** (m)	**G** (m)
(0, 0)	(0, 1)	(1.8, 1.6)	(4.5, 2)	(24.5, 2)	(24.5, 1.6)	(24.5, 0)

Figure Captions

Fig. 1. a) Location of the study area within the Chongming Dongtan wetland. b) Location of the studied tidal creek. An *Uca arcuata* crab is shown at the lower left corner. Dashed line indicates the surveyed area. c) Marsh soil stratigraphy. Soils with relatively high hydraulic conductivity were found underneath overlying mud. d) Morphology of a casted crab burrow. e) Three-dimensional schematic diagram of the modelled salt marsh. **ABCDEFG** represents the central section across the creek where crab burrows are distributed. The pore water circulation is also illustrated.

Fig. 2. Flow velocity at high tide (a, elapsed time 0 h), falling tide (b, elapsed time 3 h), low tide (c, elapsed time 6 h) and rising tide (d, elapsed time 10 h). All figures show the two-dimensional flows in the x and z direction on the central section where burrows are distributed (y = 0.25 m). The upper panel is for the case without crab burrows; and the lower panel is for the case with crab burrows. The ∇ symbol indicates the water level in the tidal creek.

Fig. 3. Time series of flow velocity at two observation points. The plot on the left hand side is for the observation point located on the left hand side of the nearest burrow to the creek (x = 4.693 m, y = 0.25 m, z = 1.725 m). The right hand side plot is for the observation point located on the right hand side of the nearest burrow to the creek (x = 4.816 m, y = 0.25 m, z = 1.725 m). a) and b) are for the case without crab burrows. c) and d) are for the case with crab burrows. The period between the two vertical dotted lines represents the emersion period.

Fig. 4. Flows in the y and z direction on the vertical along-creek section through the centre

of the nearest burrow to the creek. Results are shown for three tidal stages: falling tide (a, elapsed time 3 h), low tide (b, elapsed time 6 h) and rising tide (c, elapsed time 10 h). For comparison, flows in the x and z direction on the vertical cross-creek section through the centre of the burrow are also shown (e, f and g). Tidally averaged flows are shown in d) and h).

Fig. 5. Tidally averaged flows on the central cross-creek section (y = 0.25 m) for the case without burrows (upper panel) and with burrows (lower panel).

Fig. 6. Total water exchange volume per meter distance along the creek over a tidal cycle versus the hydraulic conductivity contrast (K_{lower}/K_{upper}).

Fig. 7. Saturation profiles in areas near the burrow next to the creek (on the central section, y = 0.25 m) at four different tidal stages: falling tide (a, elapsed time 3 h), low tide (b, elapsed time 6 h), rising tide (c, elapsed time 9 h) and beginning of overtopping (d, elapsed time 11 h). For comparison, results from the reference simulation without crab burrows are also shown (f, g, h and i). Tidally averaged saturation profiles are displayed in e) and j).

Fig. 8. Averaged saturation profiles over a tidal cycle (on the central section, y = 0.25 m) for $K_{upper} = 1.18 \times 10^{-6}$ m/s and $K_{lower} = 6.25 \times 10^{-5}$ m/s (K_{lower}/K_{upper} = 53). The upper panel is for the case without crab burrows; and the lower panel is for the case with crab burrows.

Fig. 9. Pore water pressure (head) profiles in areas below the nearest burrow to the creek (on the central section) at two different tidal stages: ebb tide (a, elapsed time 3 h) and rising tide (b, elapsed time 10 h). For comparison, results from the reference simula-

tion without crab burrows are also shown (c and d). Results are for $K_{upper} = 1.18 \times 10^{-6}$ m/s, $K_{lower} = 1.18 \times 10^{-5}$ m/s.

Fig. 10. Variations of pore water hydraulic head with time ($K_{upper} = 1.18 \times 10^{-6}$ m/s, $K_{lower} = 1.18 \times 10^{-5}$ m/s). a) is for the observation point in the upper layer (x = 4.746 m, y = 0.25 m, z = 1.7 m); and b) is for the observation point in the lower layer (x = 4.746 m, y = 0.25 m, z = 1.1 m). The period between the two vertical dotted lines represents the emersion period.

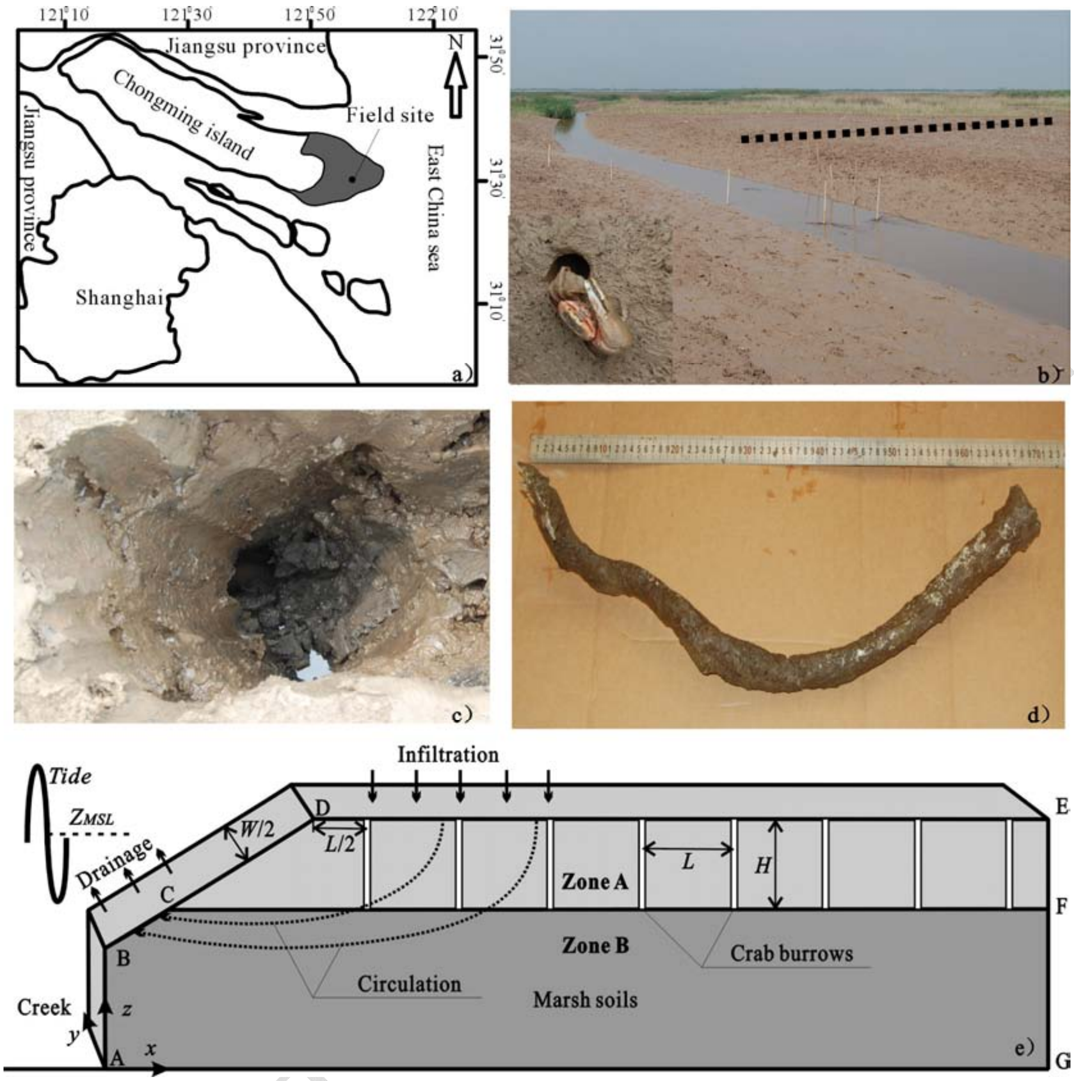
121°10′
121°30′
121°50′
122°10′
31°50′
31°30′
31°10′
N
Jiangsu province
Chongming island
Field site
Jiangsu province
East China sea
Shanghai
a)
b)
c)
d)
Infiltration
Tide
Z_{MSL}
Drainage
$W/2$
$L/2$
L
H
D
E
C
F
Zone A
Zone B
B
Crab burrows
Circulation
Marsh soils
Creek
z
y
x
A
G
e)

Fig. 1

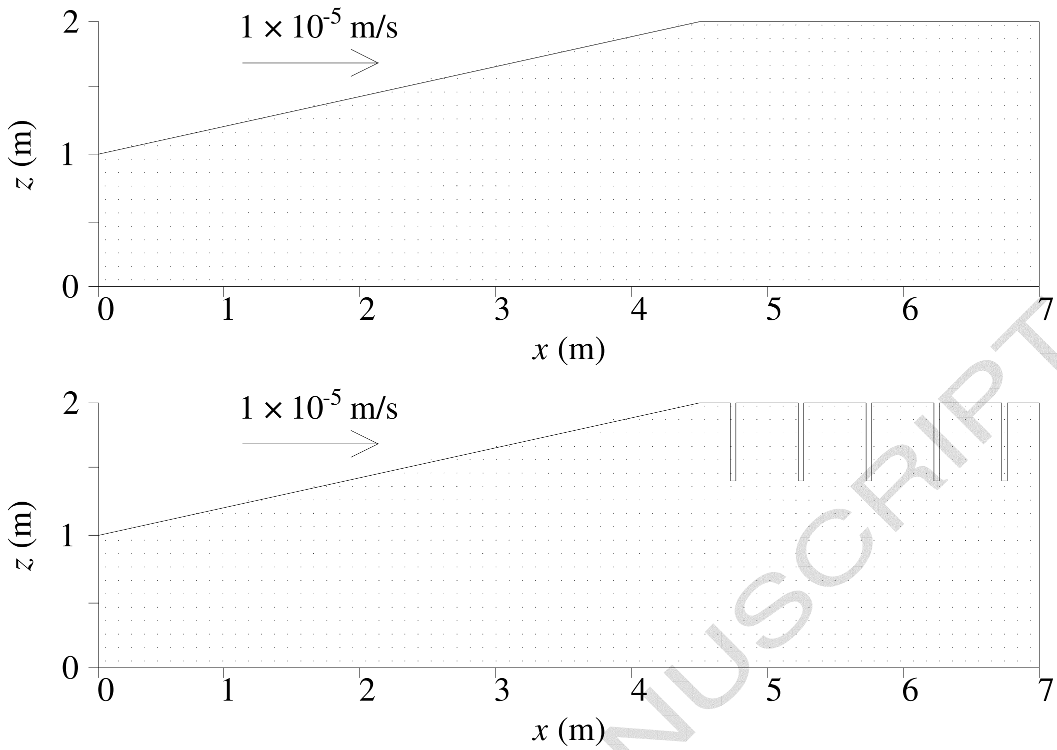

Fig. 2a

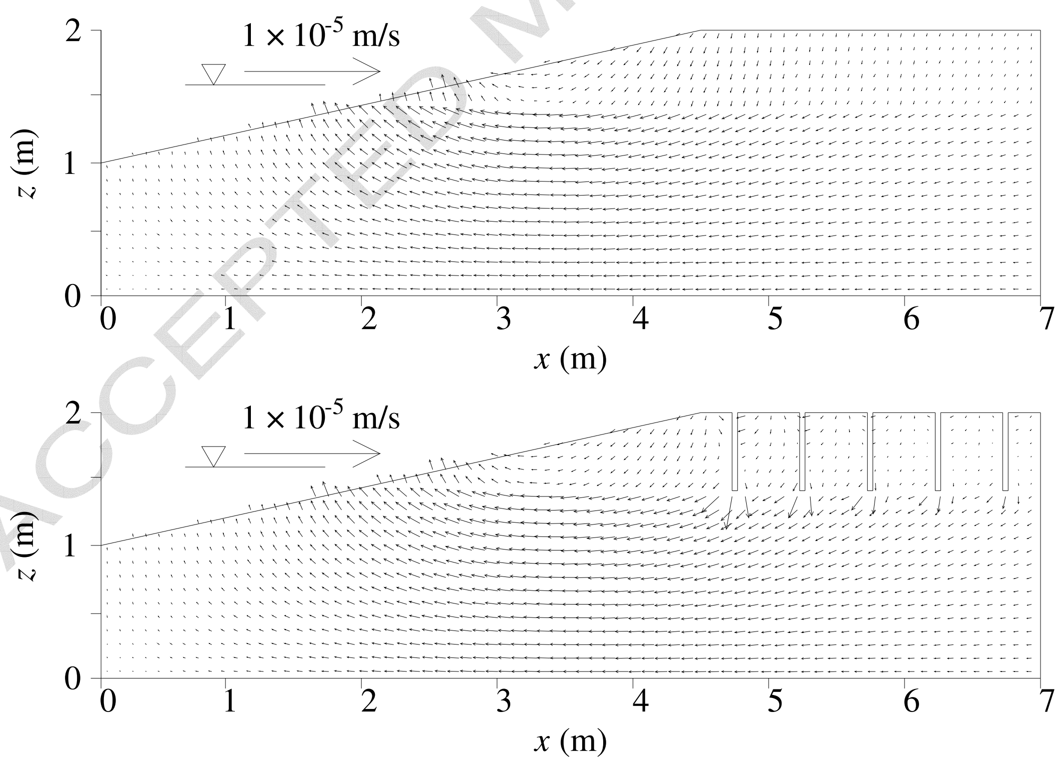

Fig. 2b

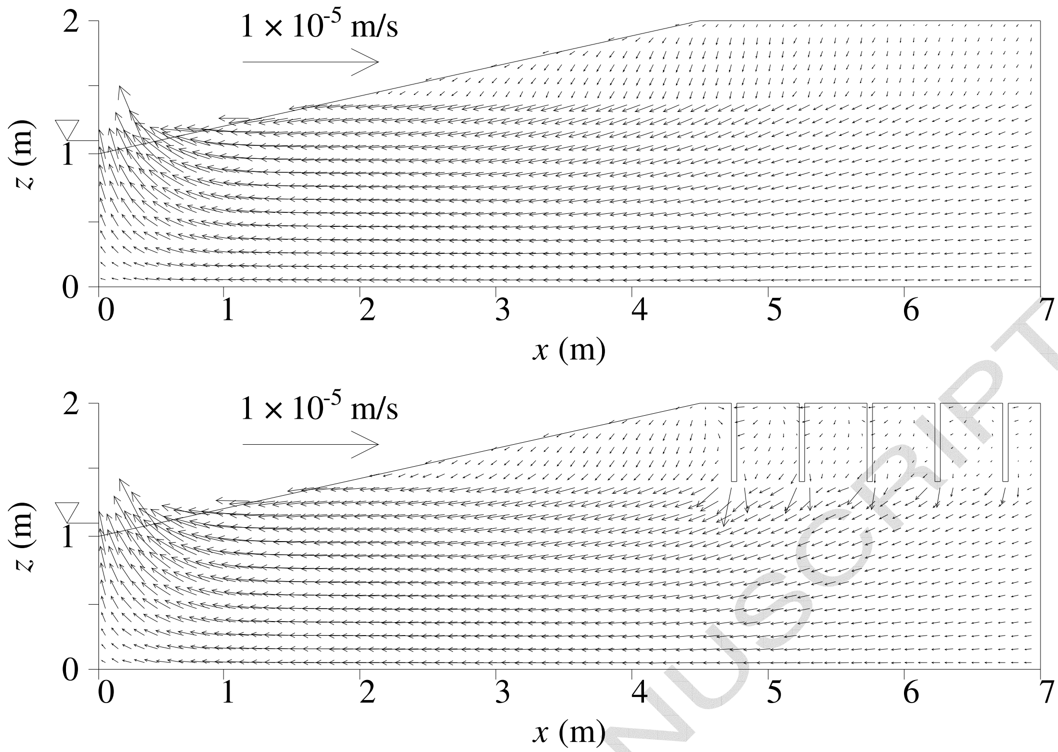
1 × 10-5 m/s
z (m)
x (m)
0
1
2
3
4
5
6
7
1 × 10-5 m/s
z (m)
x (m)

Fig. 2c

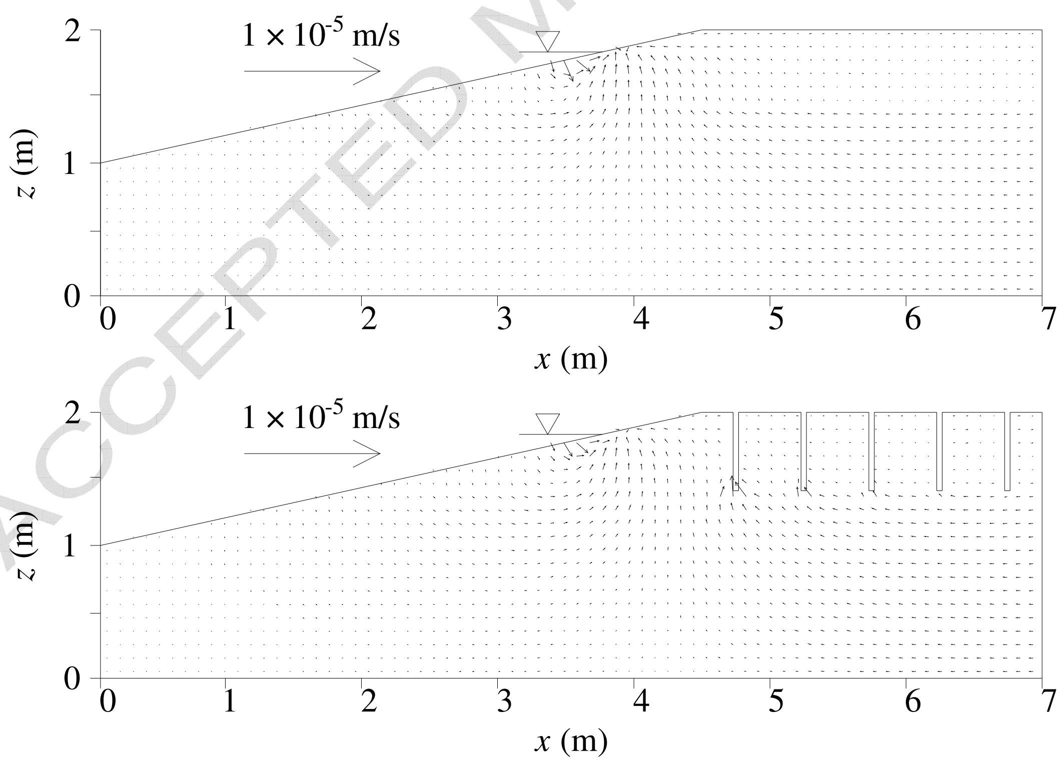
1 × 10-5 m/s
z (m)
x (m)
0
1
2
3
4
5
6
7
1 × 10-5 m/s
z (m)
x (m)

Fig. 2d

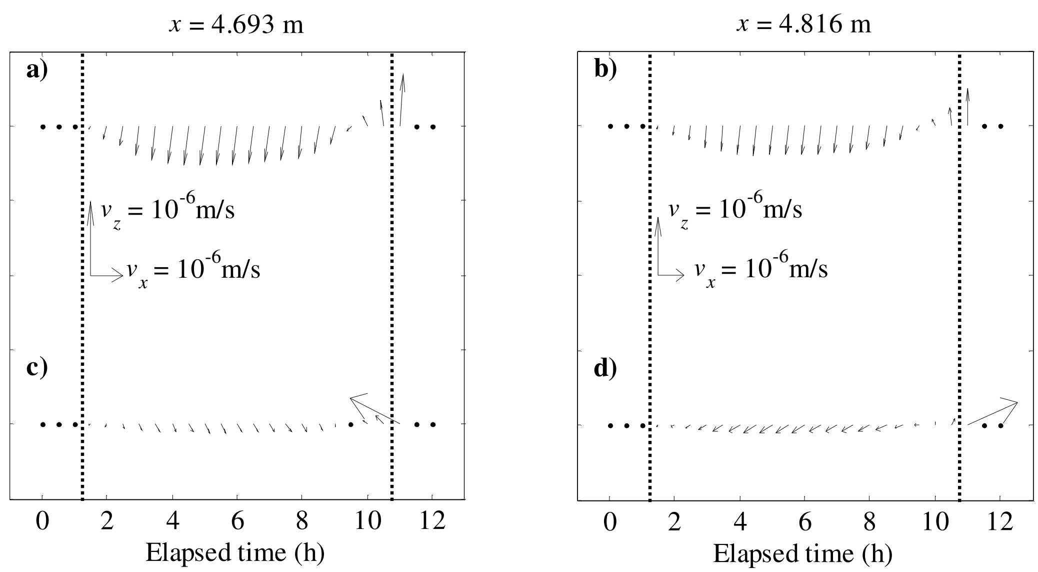
x = 4.693 m
x = 4.816 m
a)
b)
c)
d)
v_z = 10^-6 m/s
v_x = 10^-6 m/s
0 2 4 6 8 10 12
Elapsed time (h)

Fig. 3

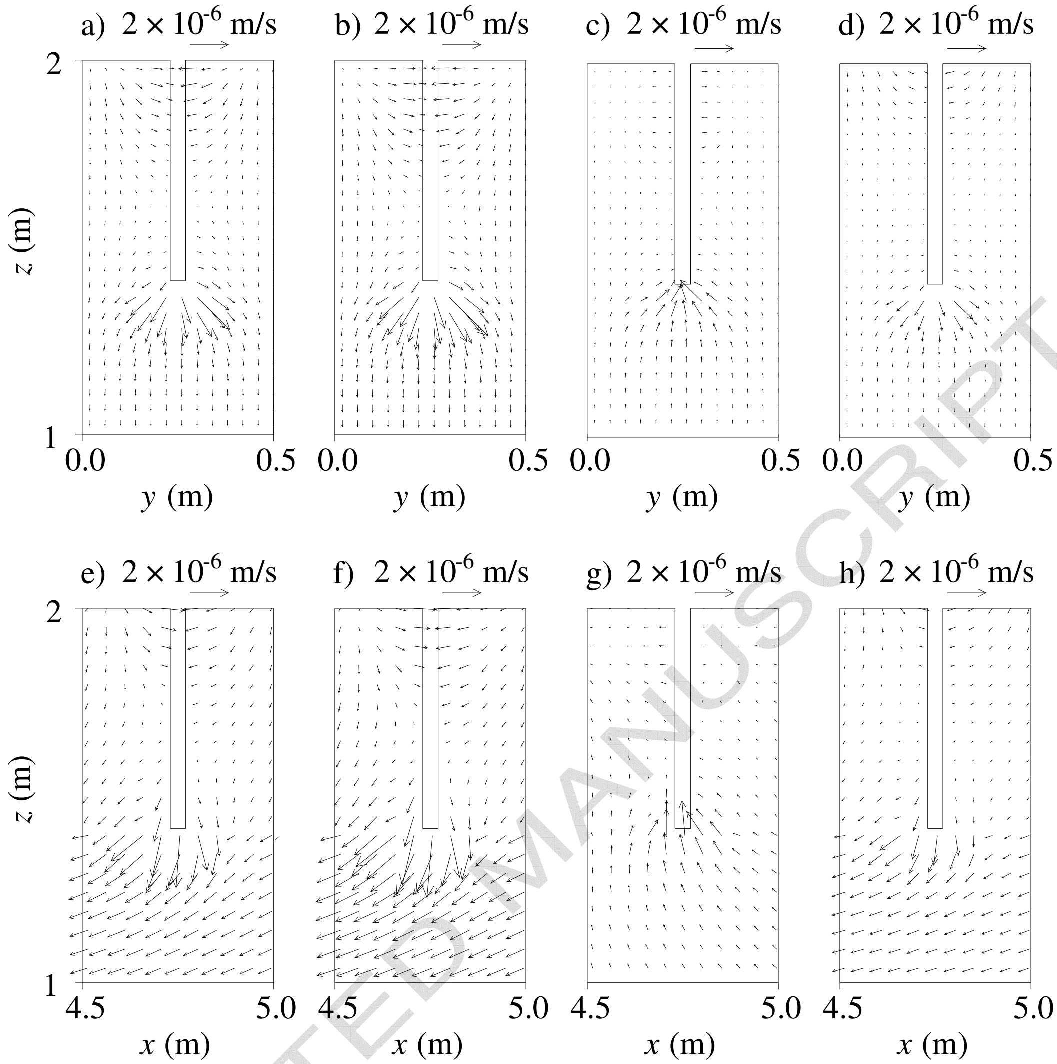
a) 2 × 10-6 m/s
b) 2 × 10-6 m/s
c) 2 × 10-6 m/s
d) 2 × 10-6 m/s
e) 2 × 10-6 m/s
f) 2 × 10-6 m/s
g) 2 × 10-6 m/s
h) 2 × 10-6 m/s
z (m)
y (m)
x (m)
0.0
0.5
4.5
5.0
1
2

Fig. 4

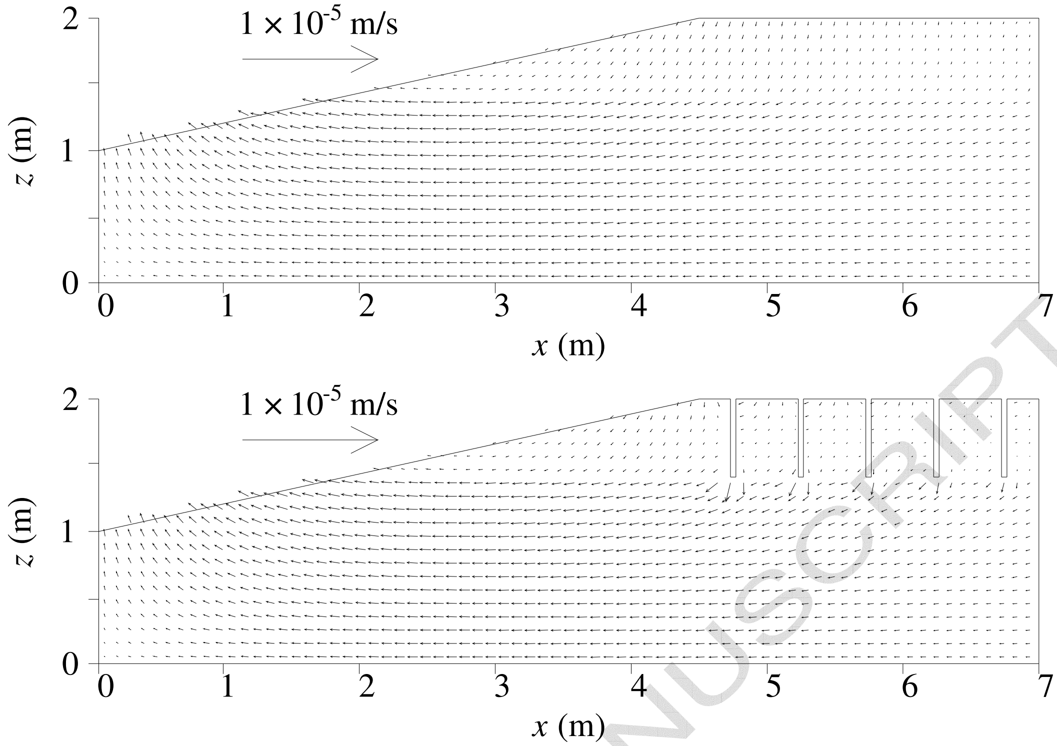

Fig. 5

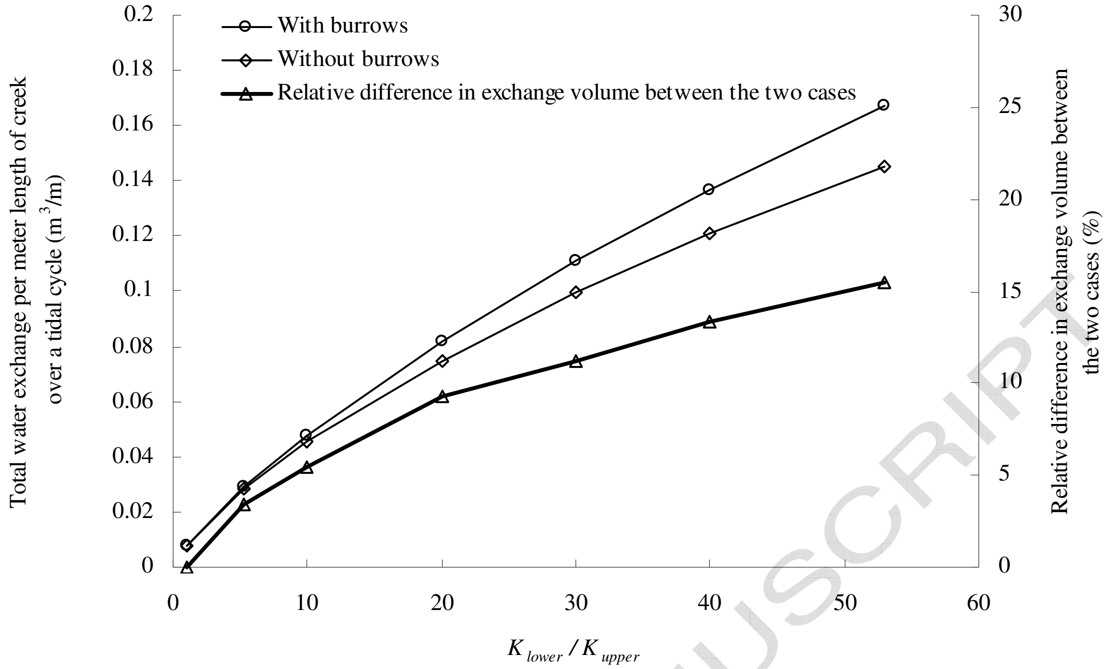

0.2
0.18
0.16
0.14
0.12
0.1
0.08
0.06
0.04
0.02
0
Total water exchange per meter length of creek over a tidal cycle (m3/m)
With burrows
Without burrows
Relative difference in exchange volume between the two cases
30
25
20
15
10
5
0
Relative difference in exchange volume between the two cases (%)
0
10
20
30
40
50
60
K lower / K upper

636

637 Fig. 6

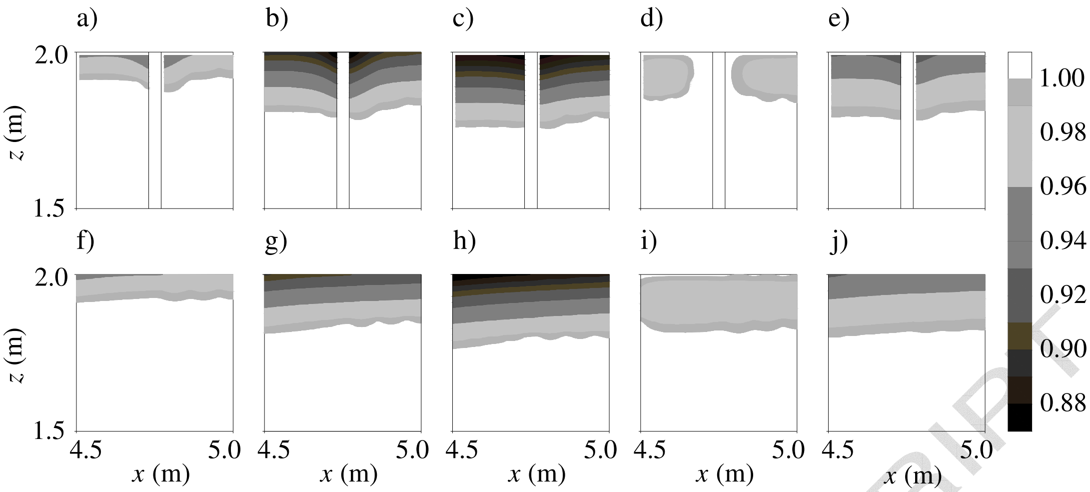

Fig. 7

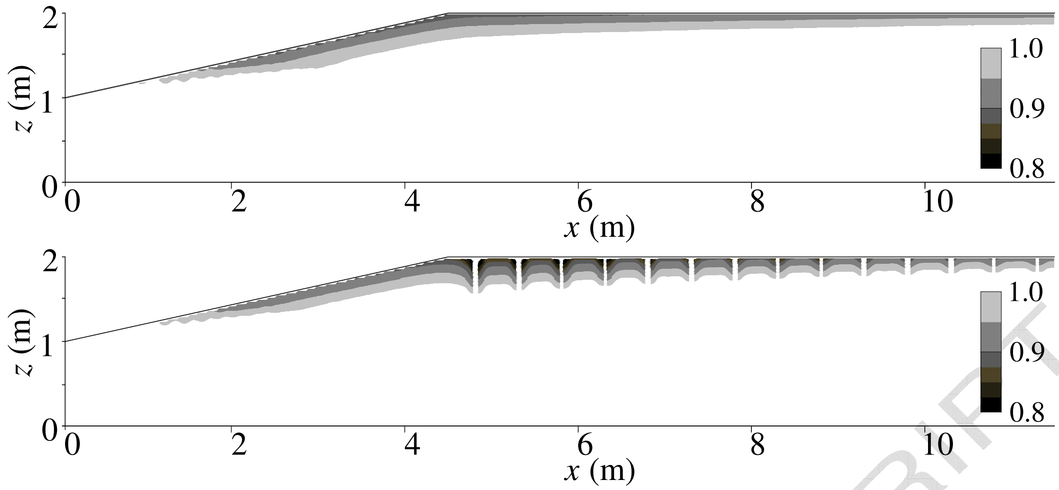

Fig. 8

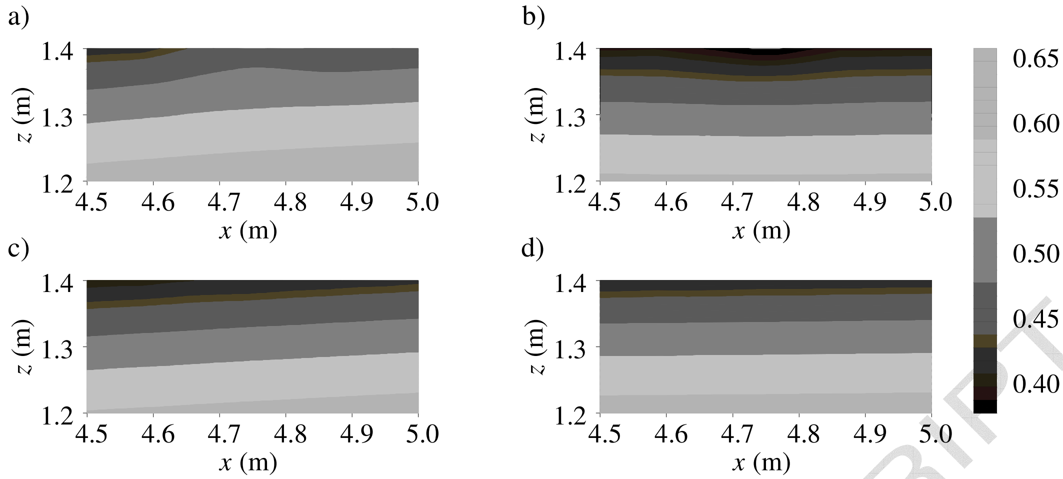

Fig. 9

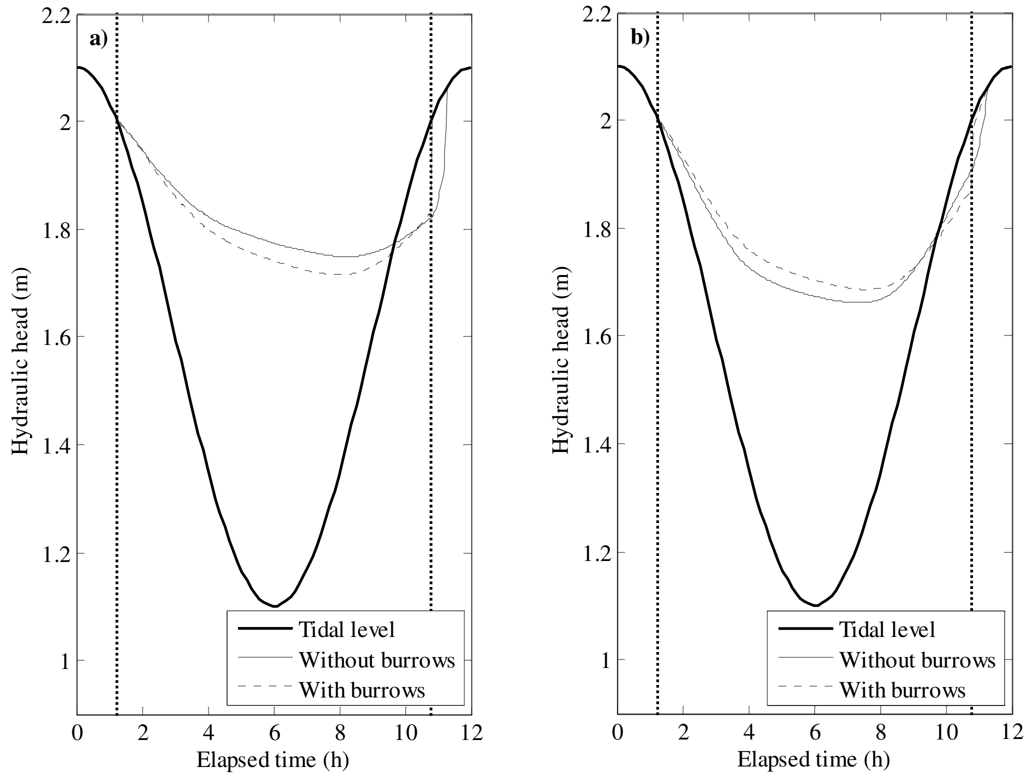

644

645 Fig. 10